Effects of Sweep, Dihedral and Skew on Aerodynamic Performance of Low-Pressure Axial Fans With Small Hub-to-Tip Diameter Ratio

Jie Wang
Department of Mechanical Engineering,
University of Twente,
P.O. Box 217,
Enschede 7500 AE, The Netherlands
e-mail: j.wang-5@utwente.nl

Niels P. Kruyt[1]
Department of Mechanical Engineering,
University of Twente,
P.O. Box 217,
Enschede 7500 AE, The Netherlands
e-mail: n.p.kruyt@utwente.nl

Axial fans with a small hub-to-tip diameter ratio are used in many branches of industry. Optimization of their aerodynamic performance is important, for which using sweep, dihedral, and skew of the blades' stacking line form an important method. Investigations on axial fans with medium to high hub-to-tip diameter ratio have shown that forward sweep of blades can give an improved aerodynamic performance, especially the total-to-total efficiency. However, only a few studies for fans with a small hub-to-tip diameter ratio have been reported. For such fans, extensive regions of backflow are present behind the fan near the hub. Based on a validated computational fluid dynamics simulation method, the effects of a sweep, dihedral and skew in axial and circumferential directions (in forward and backward direction) on the aerodynamic performance of small hub-to-tip ratio fans are investigated, with a linear stacking line. Current results show that forward sweep and circumferential skew are beneficial for higher total-to-total efficiency and that higher total-to-static efficiency can be obtained by forward dihedral and axial skew. The backward shape variety generally gives negative aerodynamic effects. Forward sweep and circumferential skew shorten the radial migration path, but more flow separation is present near the hub. With forward dihedral and axial skew, the backflow region is reduced in size and axial extent, but a more significant hub corner stall region is found. The pressure reduction due to sweep and dihedral is more limited than what could be expected from wing aerodynamics. [DOI: 10.1115/1.4051542]

Keywords: axial fans, aerodynamic performance, RANS computational fluid dynamics simulations, sweep, dihedral, skew

1 Introduction

Low-pressure axial fans with a small hub-to-tip diameter ratio (HTR in short) are widely used in many industrial and domestic applications, especially for cooling and ventilation purposes. For such fans, stators (or diffusers) are often not employed [1], due to the limited aerodynamic benefits, extra costs, and space requirements. The rotors, as key elements that determine the aerodynamic performance, have frequently been investigated, with the improvement of operational efficiency as a design objective.

The performance of an axial fan is determined by the volumetric flow rate Q and the rotational speed Ω. Performance characteristics are (total-to-static) fan static pressure rise $p_{fs} \equiv p_2 - p_{01}$, (total-to-total) fan pressure $p_f \equiv p_{02} - p_{01}$ and (input) shaft power P_{shaft}. Here p_{01} and p_{02} are the average total (or stagnation; $p_0 = p + \frac{1}{2}\rho v^2$ with v the magnitude of the absolute velocity vector) pressure at inlet and outlet, respectively, p_2 is the average static pressure at the outlet of the fan. The total-to-static efficiency η_{ts} and the total-to-total efficiency η_{tt} are defined by

$$\eta_{\text{ts}} = \frac{Q \cdot p_{fs}}{P_{\text{shaft}}} \quad \eta_{\text{tt}} = \frac{Q \cdot p_f}{P_{\text{shaft}}} \tag{1}$$

The flow rate for which the peak is attained in total-to-static efficiency η_{ts} is called the best efficiency point (BEP in short).

Dimensionless performance parameters are

$$\varphi = \frac{Q}{\frac{\pi}{8}\Omega D_{\text{fan}}^3} \quad \psi = \frac{p_{\text{fs}}}{\frac{1}{8}\rho\Omega^2 D_{\text{fan}}^2} \quad \psi_{\text{tt}} = \frac{p_{\text{f}}}{\frac{1}{8}\rho\Omega^2 D_{\text{fan}}^2} \quad \lambda = \frac{P_{\text{shaft}}}{\frac{1}{32}\rho\Omega^3 D_{\text{fan}}^5} \tag{2}$$

Here φ is the flow coefficient, ψ is the pressure coefficient, ψ_{tt} is the total pressure coefficient and λ is the power coefficient. The density of the gas is denoted by ρ and D_{fan} is the fan outer diameter (i.e., the tip diameter of the fan blades). The Reynolds and Mach numbers (based on tip radius and tip speed) are defined by

$$\text{Re} = \frac{\Omega D_{\text{fan}}^2}{4\nu} \quad \text{Ma} = \frac{\Omega D_{\text{fan}}}{2a} \tag{3}$$

where ν and a are the kinematic viscosity and the speed of sound of the gas, respectively.

The hub-to-tip diameter ratio κ is defined by

$$\kappa = \frac{D_{\text{hub}}}{D_{\text{fan}}} \tag{4}$$

where D_{hub} is the hub diameter.

Classical design methods for axial fans [1–5] are usually based on two-dimensional considerations of lift and drag coefficients of blade airfoil sections, cascade analyses, and radial equilibrium conditions to determine the stagger angles of the two-dimensional blade sections at various radial locations. To obtain the three-

[1]Corresponding author.

Contributed by the Fluids Engineering Division of ASME for publication in the Journal of Fluids Engineering. Manuscript received January 12, 2021; final manuscript received June 14, 2021; published online July 28, 2021. Assoc. Editor: Philipp Epple.

Table 1 Abbreviations for types of blade skew

	Forward	Backward
Sweep	FSW	BSW
Dihedral	FDH	BDH
Axial Skew	FAS	BAS
Circumferential Skew	FCS	BCS

dimensional blade geometry, the two-dimensional airfoil sections are stacked along a specific line, the so-called stacking line.

In conventional design methods, the simplest radial stacking line is applied, which means that the stacking points lie on a radially directed straight line.

Early research about three-dimensional stacking has been performed by Godwin [6] on compressor blades, while the first investigation for axial fan blades was by Mohammed et al. [7]. Later investigations on three-dimensional stacking lines are generally expressed in terms of sweep, dihedral, and skew. The concept of the sweep was initially introduced by Busemann [8] in 1935 in aircraft wing design to enhance drag reduction at the transonic speed [9]. For a wing with sweep, the airfoil sections are shifted in the chord direction, while with dihedral the airfoil sections are shifted in the direction perpendicular to the chord direction. Skew is a more general term, encompassing sweep as well as dihedral.

In wing aerodynamics [9,10], sweep is considered to lead to a reduction of the lift coefficient and the slope of the lift curve (with respect to that of the unswept wing) by a factor $\cos\gamma$, where γ is the sweep angle (in radians). The effect of dihedral is investigated in Ref. [11] and the corresponding lift reduction factor is $\cos^2\gamma$. A reduction in lift coefficient leads to reduced flow turning [12]. For axial fans, a similar $\cos\gamma$ effect has been reported [7,13,14].

For axial fans, the chord direction dictates sweep and dihedral (as for wings), while the absolute inflow and blade rotation directions dictate axial and circumferential skew, respectively [13,15,16]. Forward and backward sweep mean that the blade section is shifted upstream and downstream, respectively, in the relative flow field. Forward and backward dihedral and axial skew mean that the blade section is shifted upstream or downstream, respectively, of the baseline blade section in the absolute flow field. Forward or backward circumferential skew mean that the blade section is shifted in the direction of rotation or opposite, respectively. Abbreviations for the various types of blade skew are summarized in Table 1.

Mohammed et al. [7] first investigated the effects of sweep on axial fan performance for an impeller with a hub-to-tip diameter ratio $\kappa = 0.5$. Their experimental data indicate that the blades with FSW operate more efficiently than baseline (unswept) blades at low flow coefficients, while for large flow coefficients the performance of all cases is almost the same. With respect to flow fields, FSW is found to affect the blade surface velocity distribution mostly at the tip on the suction side; nearly no effects are observed at hub and midsections. For FSW, a reduction of accumulation of boundary layer flow near the tip is also found.

Subsequent investigations of the effects of sweep, dihedral, and skew reported beneficial effects, such as improvement of efficiency (η_{ts} or η_{tt}), reduction of end-wall (hub and shroud) and tip gap losses, and control of secondary flow (radial flow). Most of these advantages are found for forward types [17].

Since any shift of a blade section can be decomposed into two mutually perpendicular directions (for example, sweep can be decomposed into axial and circumferential skew), some of these benefits have common origins. Therefore, FSW and FCS are often investigated together, as in Refs. [13] and [17].

A simplified explanation of the effects of forward skewed blade effects on the velocity distribution is as follows. For FSW (and FDH, FCS, FAS) the blades near the tip protrude into the upstream flow and are able to perform work on the fluid in advance. Radial equilibrium considerations show that this leads to locally increased axial velocities near the tip and lower axial velocities near the hub. These changes in velocity fields affect flow angles, lift, and vortex distributions ($rv_{\theta 2}$) of each blade section, resulting in changed overall performance. The secondary flow downstream of blades is found to decrease (increase) by forward (backward) blade sweep, respectively [18].

Inside the blade passage, a reduction of radial accumulation of low-momentum fluid in boundary layers at the suction side surface is frequently reported [14,19–21] as the main benefit (in aerodynamic performance) from FSW and FCS. This radial migration induced by forward swept blades is illustrated in Refs. [17], [22], and [23], showing that for forward swept blades the flow path of radially outward flow near the blade surface is shortened. This is confirmed by the measured pressure distribution in Refs. [7] and [20] and the streamlines from computational fluid dynamics (CFD for short) simulations in Refs. [14] and [21] near the blade suction side surface. Therefore, the accumulation of low-momentum fluid near the tip is reduced, and the associated reduction of end-wall and the tip losses both contribute to the improvement of efficiency [19]. A reasoning analogous to the one that explains the benefits of forward-swept blades shows that backward-swept blades are less favorable for the improvement of aerodynamic performance [14].

Yet, there is no universal conclusion on how these blade shapes can influence the aerodynamic performance of all axial fan blades, as noted by Vad in his remarkable overviews [17,23]. In comparison to a baseline case, FSW gave an increased η_{tt} in Ref. [19], unchanged η_{ts} in Ref. [13], and decreased η_{tt} in Ref. [24]. For BSW, studies reported increased η_{tt} in Ref. [25] as well as decreased η_{tt} in Ref. [24]. Note that these results have been reported for different blades and different flow coefficients.

With respect to dihedral, effects similar to those for sweep (efficiency gain [15,26], reduction of tip losses, and unloading of the tip [27]) have been reported. Furthermore, FDH is reported to suppress secondary flow and delay corner stall [28], while BDH gives opposite effects [29]. In Ref. [30], FDH with a large angle (45 deg) is found to eliminate stall in an axial fan with $\kappa = 0.5$, while η_{tt} is decreased at high flow rates.

The forward and backward swept blades referred to above are mainly FSW, FDH, FCS, and BSW, BDH. Investigations of BCS and axial skew are rarely reported. Since circumferential skew involves a sweep component, FSW and FCS are usually discussed together, while BSW and BCS are less interesting. As for axial skew, it is only reported in Ref. [21], with FAS compared to FSW, without reference to BAS.

The analyses of the effects of sweep generally focus on total-to-total efficiency and total-to-total pressure rise, while effects on total-to-static efficiency and total-to-static pressure rise are only reported in few studies.

The hub-to-tip diameter ratio κ of the axial fans in the above mentioned investigations are all medium to high, with some examples listed in Table 2. Studies of axial fans with small HTR ($\kappa \leq 0.2$) are rarely found. As shown in Refs. [14] and [21], radial outward flow occurs nearly over the whole blade surface from hub to tip. This is not likely to occur for fans with small HTR where the chord of the blade sections is relatively smaller. Another

Table 2 Hub-to-tip diameter ratio κ of example axial fans

Reference	Beiler [13]	Hurault [18]	Mohammed [7]	Ramakrishna [21]	Vad [24]	Corsini [19]
$\varkappa$	0.4	0.45	0.5	0.5	0.5	0.68

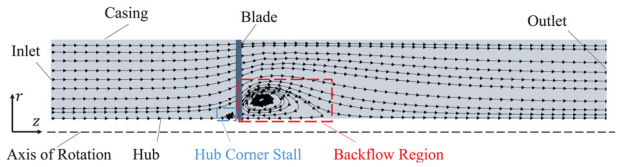

Fig. 1 CFD results for the streamlines in the meridional plane: backflow region and hub corner stall of Howden fan at best efficiency point [31]

important characteristic of such fans is that backflow occurs downstream of the fan blades [1,4]. To the best of the authors' knowledge, the effects of the sweep, dihedral, and skew on the backflow region have not been reported in the literature.

The focus of this study is on a baseline Howden axial fan with small HTR ($\kappa = 0.14$) and as shown in Fig. 1, extensive backflow together with hub corner stall is present downstream and upstream of the blades for such this fan [31].

The main aim of this study is to investigate the effects of the sweep, dihedral, and skew on the aerodynamic performance of low-pressure axial fans with a *small hub-to-tip ratio* κ. CFD simulations are employed since it is (relatively) easy to change the blade geometry and determine the resulting overall aerodynamic performance as well as investigate corresponding flow fields. As discussed above, the advantages and disadvantages of sweep and dihedral can also be utilized via circumferential skew and axial skew. Therefore, the investigations of sweep and dihedral are reported as focal points, with some investigations of skew to strengthen the results. Since the operation range of the investigated low-pressure axial fan with small HTR is outside of the stall range, this study focuses on flow rates near the best efficiency point BEP and on large flow rates.

Specific objectives of this CFD study are to study the effects of the sweep, dihedral, and skew on:

- Total-to-total and total-to-static pressure and efficiency;
- Hub corner stall and backflow region near BEP;
- Flow fields near the blade surface and in the blade-to-blade view, close to BEP;
- Reduction of the pressure coefficient due to sweep and dihedral.

It should be noted that the objective of this study is not to perform an optimization but to study the effects of the sweep, dihedral, and skew on the aerodynamic performance of low-pressure axial fans with small HTR. Therefore, neither structural mechanics nor aeroacoustic effects are considered, although sweep is often employed to reduce noise.

The outline of this study is as follows. The geometry of the baseline fan with small HTR as well as that of the fans with sweep, dihedral, and skew are described in Sec.2. A CFD simulation strategy validated in Ref. [31] is summarized in Sec. 3. The predicted aerodynamic performances and flow field analyses are presented in Sec. 4. An overview of the effects of the sweep, dihedral and axial, and circumferential skew are given in Sec. 5. Finally, conclusions and recommendations are formulated in Sec. 6.

2 Geometry of Baseline Fan and Definition of Sweep, Dihedral, and Skew

The baseline Howden fan for this research is described in detail in Ref. [31]. Of each of the six identical blades only the "main" [31], airfoil-shaped blade is considered here. The airfoil sections correspond to the Wortmann profile [32], with a chord length of 0.15 m. The sections are slightly twisted (by 4 deg) and with a rounded trailing edge shape. The stagger angle χ of the baseline fan ($\chi = 15$ deg) is defined in Fig. 2(*a*). The stacking point of each spanwise location is the maximum thickness point. The stacking line of the baseline fan is radially straight, see also Fig. 2(*b*). The

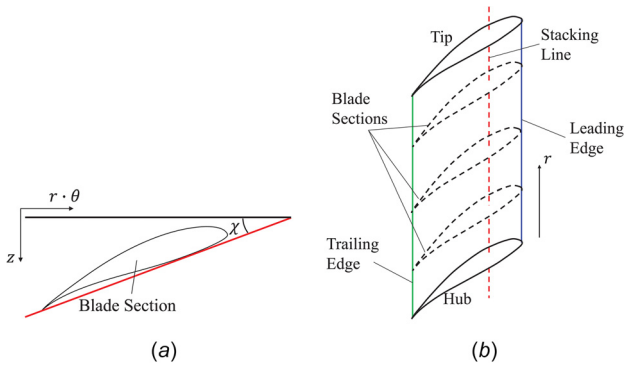

Fig. 2 Geometrical description of (*a*) stagger angle χ and stagger line (in red), (*b*) sketch of the main blade of the baseline fan, with blade sections, stacking line (in red, tangential to the pressure side of the blade), leading and trailing edges (in blue and green, respectively); r, z, θ represent the radial, axial and circumferential directions

Table 3 Geometrical and design parameters of the baseline fan [31]

Rotational speed (rpm)	497
D_{fan} (m)	1.829
κ	0.14
Number of blades	6
Stagger angle (deg)	15
Chord length of main blade (m)	0.15

main geometrical and design parameters of the baseline fan are summarized in Table 3.

By changing the stacking line (and keeping the shape of the blade sections the same), sweep, dihedral and skew can be applied to the baseline fan blade. In a cylindrical coordinate system, r, θ, z indicate the radial, circumferential and axial locations, corresponding to spanwise, rotation, and absolute inflow directions. With sweep, the stacking line is shifted parallel to the chord line. The stagger line (red line in Fig. 2(*a*) that is tangential to the

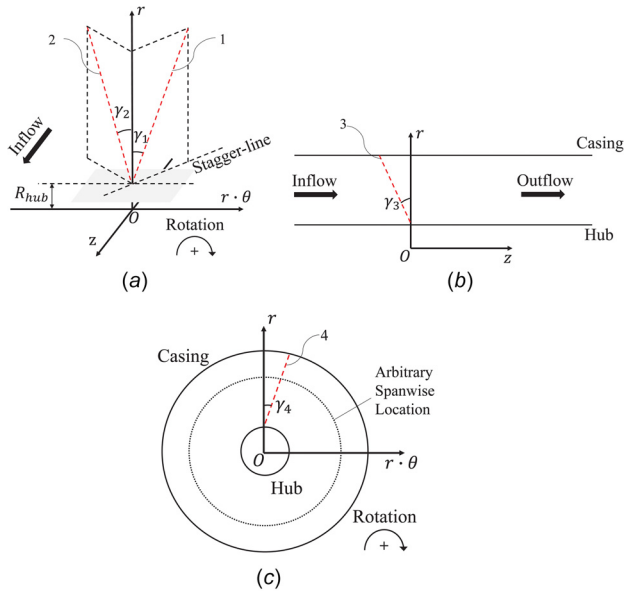

Fig. 3 Geometrical description of (*a*) stacking line for sweep and dihedral (in red and denoted by "1" and "2," respectively) and angles γ_1 and γ_2 (*b*) stacking line for axial skew (in red and denoted by "3") and angle γ_3, and (*c*) stacking line for circumferential skew (in red and denoted by "4") and angle γ_4

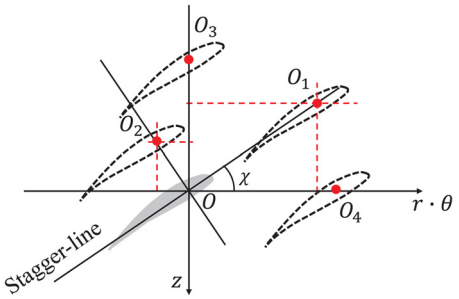

Fig. 4 Geometrical description of blade section shift: O, O_1, O_2, O_3, and O_4 represent stacking points of original blade, and blades with (forward) sweep and dihedral, axial and circumferential skew, respectively. Inflow is in the positive *z*-direction.

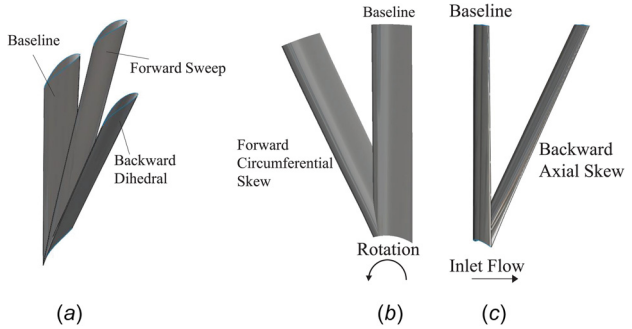

Fig. 5 Example blades of baseline case and (*a*) FSW and BDH, (*b*) FCS, and (*c*) BAS

pressure side of the blade section) is used here (instead of the chord line) as a reference for the sweep. Dihedral means that the stacking line is shifted in the direction that is perpendicular to the direction of sweep. Axial and circumferential skew mean that the stacking line is shifted in axial and circumferential direction, respectively.

The stacking line of the baseline fan is radially straight. Here blades with sweep, dihedral, and skew are considered where the stacking line is *straight* (but not radial as for the baseline fan). The stacking lines are then characterized by a single angle (γ_1 for a sweep, γ_2 for dihedral, γ_3 for axial skew, and γ_4 for circumferential skew). Examples of stacking lines and corresponding angles of sweep, dihedral, axial, and circumferential skew are shown in Figs. 3(*a*)–3(*c*).

The change of the stacking line results in a shift of the location of the stacking points of the blade sections on the Blade-to-blade (B2B in short) surface. The blade section shifts of sweep, dihedral, and skew in the B2B view are shown in Fig. 4 with O, O_1, O_2, O_3, and O_4 representing the stacking point of the blade sections for baseline case and cases with sweep, dihedral, axial, and circumferential skew, respectively.

Cases of the sweep, dihedral, axial, and circumferential skew, forward as well as backward, have been investigated; the angles $\gamma_1, \gamma_2, \gamma_3, \gamma_4$ range from −25 deg to 25 deg (with 5 deg increment). Examples of the baseline fan blade (for which $\gamma_1 = \gamma_2 = \gamma_3 = \gamma_4 = 0$ deg), and blades with FSW, BDH, FCS, and BAS are shown in Fig. 5.

3 Computational Fluid Dynamics Simulation Strategy

In the CFD simulations for low-pressure axial fans with a small hub-tip ratio in Ref. [31] special attention was paid to trailing edge shape, presence of nonaerodynamically shaped blade sections, tip gap, and employed turbulence model. Here their CFD simulation strategy is adopted that gave good agreement between experimental aerodynamic performance (pressure rise as well as total-to-static efficiency) and corresponding CFD predictions.

The flow is considered as being effectively incompressible due to the low speeds (Ma < 0.15). Only a single blade passage is modeled since diffuser blades are absent. In the frame of reference that is rotating with the fan blades, the flow is considered to be steady. The computational domain is extended by one and two casing diameters upstream and downstream from the blades, respectively, to reduce the influence of imposed boundary conditions at the inlet and outlet on the CFD results. The tip gap is not taken into consideration to simplify the simulations and to limit the required mesh size. The computational domain is shown in Fig. 6.

The turbulent, Reynolds-averaged flow field is described by the continuity equation and Reynolds-averaged Navier–Stokes (RANS) momentum equations

$$\frac{\partial \overline{v}_i}{\partial x_i} = 0 \qquad \frac{\partial \overline{v}_i}{\partial t} + \frac{\partial (\overline{v}_i \overline{v}_j)}{\partial x_j} = -\frac{1}{\rho}\frac{\partial \overline{p}}{\partial x_i} + \nu \frac{\partial^2 \overline{v}_i}{\partial x_j \partial x_j} - \frac{\partial \left(\overline{v_i' v_j'}\right)}{\partial x_j} + g_i \tag{5}$$

Here $\overline{v}_i$ is the Reynolds-averaged (absolute) velocity vector, x_i denotes the ith spatial coordinate, $\overline{p}$ is the Reynolds-averaged pressure, v_i' is the velocity fluctuation and $-\rho \overline{v_i' v_j'}$ is the Reynolds stress tensor and ρg_i denotes a body force. The Einstein summation convention has been employed, implying a summation over repeated subscripts. The Reynolds stress tensor is modeled by the Boussinesq eddy-viscosity hypothesis, with the Spalart–Almaras model [33] as a single-equation model for the turbulent viscosity. This turbulence model gave the most accurate results in Ref. [31] for the considered baseline fan with small HTR.

As boundary conditions, the inlet flow is assumed as being uniform and with no preswirl and low turbulence level. Furthermore, at the inlet and outlet the total pressure and flow rate are prescribed, respectively. At the outlet, the pressure distribution conforms to the radial equilibrium condition. No-slip conditions are applied on the blade, hub, and casing surfaces. The hub and blade surfaces have the same rotational speed. Periodic boundary conditions are applied in the circumferential direction at the corresponding surfaces.

Based on the grid convergence analyses presented in Ref. [31], multiblock structured meshes have been generated with about 1.5×10^6 grid points. The steady RANS flow equations are discretized with a cell-centered second-order finite volume approach.

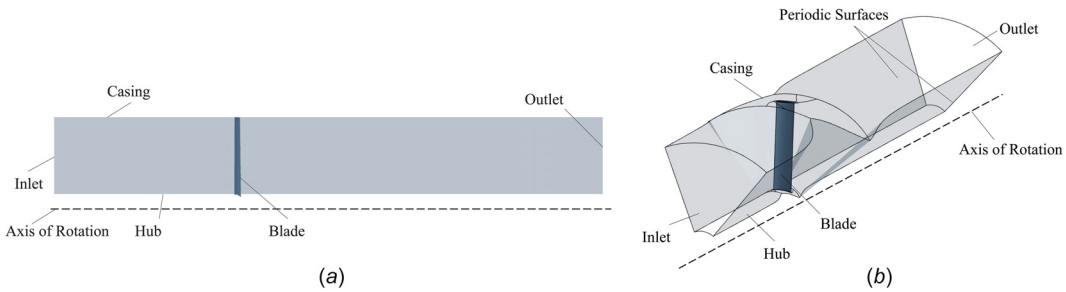

Fig. 6 Computational domain: (*a*) meridional view and (*b*) three-dimensional view

The discretized nonlinear equations have been solved iteratively, with a reduction in global residual by six orders of magnitude used as a convergence criterion.

This simulation strategy is applied in all CFD simulations involving forward and backward sweep, dihedral, and axial and circumferential skew. The results are presented in Sec. 4.

4 Predicted Aerodynamic Performance

The CFD results for the baseline fan are compared to the fans with skewed blades to investigate the effects of the sweep, dihedral, and skew on the aerodynamic performance, in Secs. 4.1–4.4, respectively. The aerodynamic performance curves are shown first, followed by the analyses of the flow fields to better understand the origins of the observed effects.

To avoid too much overlap of performance curves, results are shown for sweep angles of 5 deg, 15 deg, and 25 deg. The discussed overall aerodynamic parameters are pressure coefficient ψ, total pressure coefficient ψ_{tt}, total-to-static efficiency η_{ts} and total-to-total efficiency η_{tt}. Six flow coefficients are considered: low flow coefficient (φ near 0.11), near BEP (φ near 0.13 and 0.15) and larger flow coefficients (φ near 0.19, 0.21, and 0.23). The performance curves are created by cubic spline interpolation through the six CFD predicted points. Since the resulting characteristics of ψ and ψ_{tt} are nearly the same, only the results for ψ are shown.

4.1 Sweep. The results for sweep are reported first. As described in Ref. [23], outward radial fluid migration for nonfree vortex designs can be moderated via FSW to reduce losses. Thus, the combination of FSW and a nonfree vortex distribution has been recommended to obtain improved performance. The vortex distribution of the baseline fan strongly differs from a free-vortex design (as shown in Fig. 9 of Ref. [31]). Therefore, improved aerodynamic performance is expected from FSW, relative to the baseline fan. With respect to the pressure coefficient, it could be expected that a reduction by a factor $\cos\gamma$ is observed.

The predicted aerodynamic performance of fan blades with a forward sweep (FSW) for different sweep angles is shown in Fig. 7.

Contrary to expectation, the pressure coefficient ψ is hardly affected by FSW for the BEP flow coefficient (φ near 0.15) and larger (see Fig. 7(*a*)). For a small flow coefficient φ, only for a sweep angle of 25 deg a decrease is observed (by a factor of 0.96; much less than expected from the $\cos\gamma$ effect).

The total-to-static efficiency η_{ts} decreases with increasing FSW sweep angle for the low flow coefficient φ near 0.11 (maximum drop by 1.87% for 25 deg FSW), see Fig. 7(*b*). Modest improvements are noted near BEP and for large φ. Near BEP, the largest improvement is 0.33% for 15 deg FSW. At large φ near 0.23, the maximum increase is 1.21% for 25 deg FSW.

With increasing FSW, the total-to-total efficiency η_{tt} decreases at low flow coefficient φ and increases at high flow coefficient φ, see Fig. 7(*c*). The maximum drop (1.82%) and improvement (1.19%) are both obtained for 25 deg FSW at low and high φ, respectively. Near BEP, the predicted performance is effectively not affected by FSW. Overall, fan blades with FSW give

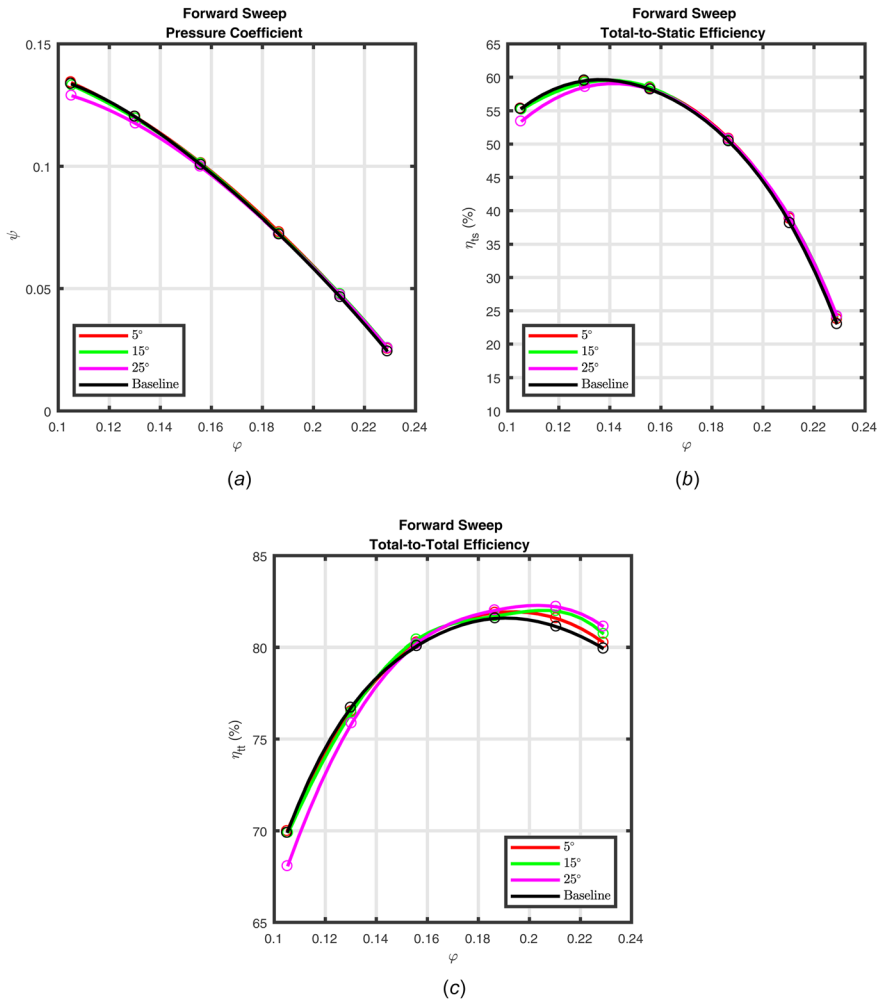

Fig. 7 CFD Predictions: comparison between baseline fan and fans with FSW: (*a*) static pressure coefficient ψ, (*b*) total-to-static efficiency η_{ts}, and (*c*) total-to-total efficiency η_{tt}: (*a*) $\varphi-\psi$, (*b*) $\varphi-\eta_{ts}$, and (*c*) $\varphi-\eta_{tt}$

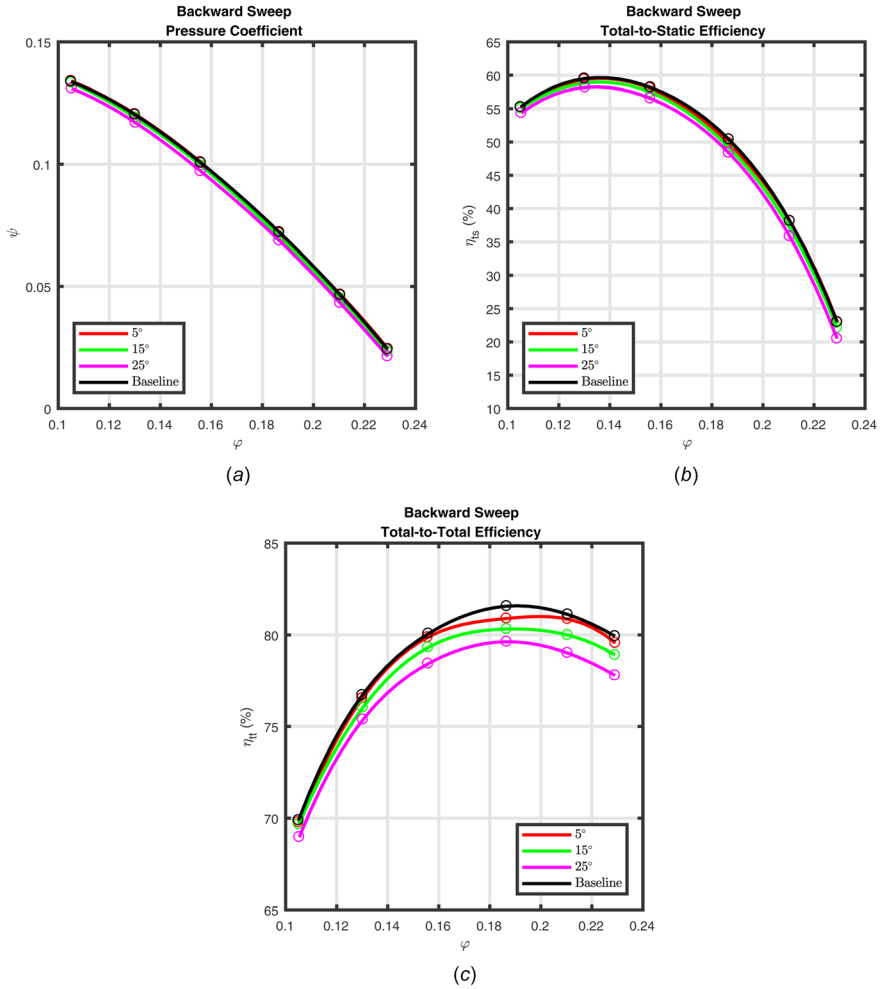

Fig. 8 CFD predictions: comparison between baseline fan and fans with BSW: (*a*) pressure coefficient ψ, (*b*) total-to-static efficiency η_{ts}, and (*c*) total-to-total efficiency η_{tt}: (*a*) $\varphi-\psi$, (*b*) $\varphi-\eta_{ts}$, and (*c*) $\varphi-\eta_{tt}$

improved η_{tt} at large flow coefficients, while limited benefits are obtained near BEP.

Contrary to FSW, BSW does not give benefits, as shown in Fig. 8. A larger BSW angle results in a larger decrease of the pressure coefficient ψ, the total-to-static efficiency η_{ts} as well as the total-to-total efficiency η_{tt}. The drop in ψ and η_{ts} does not vary much with flow coefficient φ. However, for η_{tt}, larger decreases are found for large φ. Near BEP, the maximum drop (for 25 deg BSW) in ψ is 3.4%, and the drops in η_{ts} and η_{tt} are 1.7% and 1.6%, respectively.

For the baseline fan at large flow coefficient $\varphi = 0.23$, secondary flow and backflow are almost eliminated [31]. To investigate the influence of sweep on the downstream backflow region and radial migration near the blade surface, the flow field analyses focus on streamlines in the meridional plane and near the blade suction side surface at BEP. In particular, the occurrence of the hub corner stall and the backflow region are investigated, see also Fig. 1. The cases of FSW and BSW with a maximum angle of 25 deg are investigated to have a clearer view of the influence of sweep on the flow field.

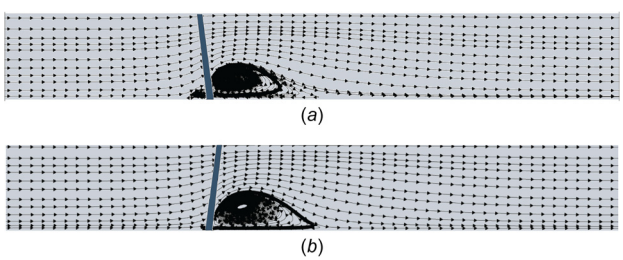

Fig. 9 Comparison of meridional surface streamlines: (*a*) 25 deg FSW and (*b*) 25 deg BSW; both for flow coefficient at BEP

The streamlines in the meridional plane for 25 deg FSW and 25 deg BSW are shown in Fig. 9. The downstream backflow region with BSW blades is larger than that with FSW blades. However, the upstream hub corner stall region with BSW blades is smaller than that with FSW blades. More intensive connections between the hub corner stall and backflow regions are found with FSW blades, which may give more losses that reduce the improvement in aerodynamic performance expected with FSW blades.

The streamlines of the relative flow at BEP near the blade suction side surface (inside the boundary layer; at the averaged value of $y^+_{avg} = 8.7$) are compared in Fig. 10 for the baseline blade, and blades with 25 deg FSW and 25 deg BSW. Here the view is in the axial direction, from the inlet toward outlet. Radial outward flow is present for all cases, which starts from the hub toward the midspan of the blade and collects near the trailing edge. For the baseline case and BSW, the radial flow develops toward the tip, but for FSW there are even some streamlines from the tip toward the lower span at the trailing edge. The main streamlines occupy most

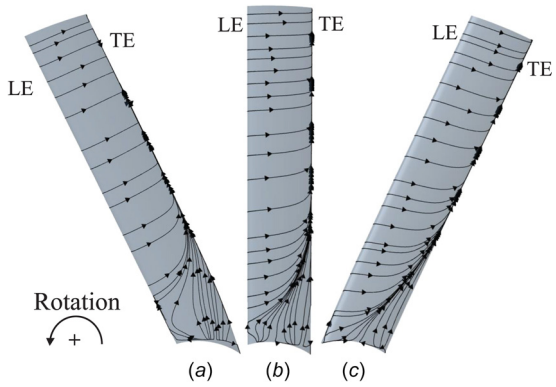

Fig. 10 Boundary layer streamlines near blade suction side surface for (*a*) 25 deg FSW, (*b*) baseline, and (*c*) 25 deg BSW; All for flow coefficient at BEP, "LE" and "TE" stand for leading and trailing edge

area of the blade surface, which is different from what is found in Refs. [14] and [21] (where κ equals 0.4 and 0.5, respectively). Overall, the radial outward flow path is reduced by FSW, and the radial outward flow region is limited for these fans with small HTR.

In both Figs. 9(*a*) and 9(*b*), the corner vortex is present near the hub. The relative velocity streamlines in the B2B view at 2.5% spanwise location are shown in Fig. 11. For both baseline case and BSW, only a vortex near the trailing edge is found, but with FSW a vortex near the leading edge is also found, corresponding to the more intensive hub corner stall also shown in Fig. 9.

Therefore, sweep applied to axial fans with a small hub-to-tip ratio will give minor improvements in pressure coefficient ψ and total-to-static efficiency η_{ts} over the full range of flow coefficient φ, but FSW is helpful to obtain higher total-to-total efficiency η_{tt} at large φ. With respect to the velocity distribution, although sweep clearly affects the radial migration, the affected area is quite small, which therefore hardly contributes to the overall aerodynamic performance. The flow field analyses have shown that FSW is able to reduce the downstream backflow region (BSW has the opposite effect), yet more intensive upstream hub corner stall is also found for FSW.

4.2 Dihedral. With dihedral, the stacking line is shifted in the direction perpendicular to the chord line. FDH has been reported to give increased total-to-total efficiency (by 1.33%) [26] and to affect the velocity distribution downstream of the fan blades [28]. Also, BEP is shifted toward a lower flow coefficient φ by FDH. An extreme case (with a large dihedral angle of 45 deg) is considered in Ref. [30], where FDH eliminates the stall in the operation range. As for the reduction in lift coefficient, different from sweep, a factor $\cos^2\gamma$ has been reported in Ref. [11] for wings.

The predicted aerodynamic performance of fan blades with FDH for different dihedral angles is shown in Fig. 12.

For the pressure coefficient ψ, a decrease in ψ is found with FDH. This reduction increases with FDH angle. The maximum decrease is 22% with 25 deg FDH for flow coefficient $\varphi = 0.23$.

For the total-to-static efficiency η_{ts}, blades with 5 deg–25 deg FDH give improvements at low flow coefficients φ, the maximum increase is 0.95% found for 15 deg FDH near $\varphi = 0.11$; at flow coefficients φ larger than BEP, 5 deg FDH gives nearly the same efficiency as the baseline case, while others result in drops; the maximum drop is found at $\varphi = 0.23$ for 25 deg FDH.

With respect to the total-to-total efficiency η_{tt}, blades with 5 deg–15 deg FDH perform better for all flow coefficients φ; 25 deg FDH performs better only at low φ. The largest improvement is 0.82% with 15 deg FDH near $\varphi = 0.11$; this is the same as what has been found for η_{ts}.

Therefore, considering the improved, higher η_{ts} and η_{tt}, 15 deg performed better among all FDH. Larger dihedral angles are not recommended due to large drops in both ψ and η_{ts}.

The predicted aerodynamic performance of fan blades with BDH for different angles shows significant decreases in aerodynamic performance (data not shown), with larger dihedral angles giving larger decreases. 5 deg BDH gives nearly the same performance as the baseline case; all other BDH result in decreased performance over all φ. The maximum drops in pressure coefficient ψ, total-to-static efficiency η_{ts} and total-to-total efficiency η_{tt} are for 25 deg BDH.

According to Ref. [28], FDH is able to suppress secondary flow. To investigate the effects of dihedral on the hub corner stall and backflow, the streamlines in the meridional plane are shown in Fig. 13 for 25 deg FDH and 25 deg BDH at flow coefficient φ near BEP. FDH (slightly) intensifies the hub corner stall upstream of the blade and reduces the backflow region downstream of the blade; the opposite effects are found with BDH.

The relative velocity streamlines near the blade suction side surface are shown in Fig. 14 for 25 deg FDH and 25 deg BDH and are compared with the baseline case for flow coefficient φ near BEP. The streamlines are different from those for sweep cases in Fig. 9, no significant difference in radial outward flow pattern is found between FDH and BDH blades, but the extent of radial flow is reduced in comparison to the baseline case.

A visualization of the relative velocity streamlines in the B2B view at 2.5% spanwise location, for both baseline case and BDH, showed that only a vortex near the trailing edge is found at the hub (data not shown). For FDH a small vortex near the midchord is also found, which corresponds to a slightly more intensive hub corner stall region.

Although higher total-to-total efficiency η_{tt} can be obtained from 15 deg FDH, the overall aerodynamic performance of fan blades with dihedral is not satisfactory, since no significant improvement in total-to-static efficiency η_{ts} is obtained.

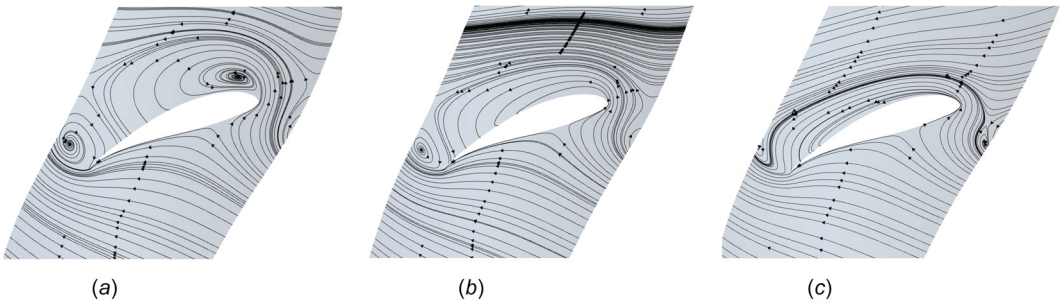

Fig. 11 Velocity streamlines based on the relative velocity in the blade-to-blade plane at 2.5% spanwise location for: (*a*) 25 deg FSW, (*b*) baseline case, and (*c*) 25 deg BSW; all for flow coefficient near BEP

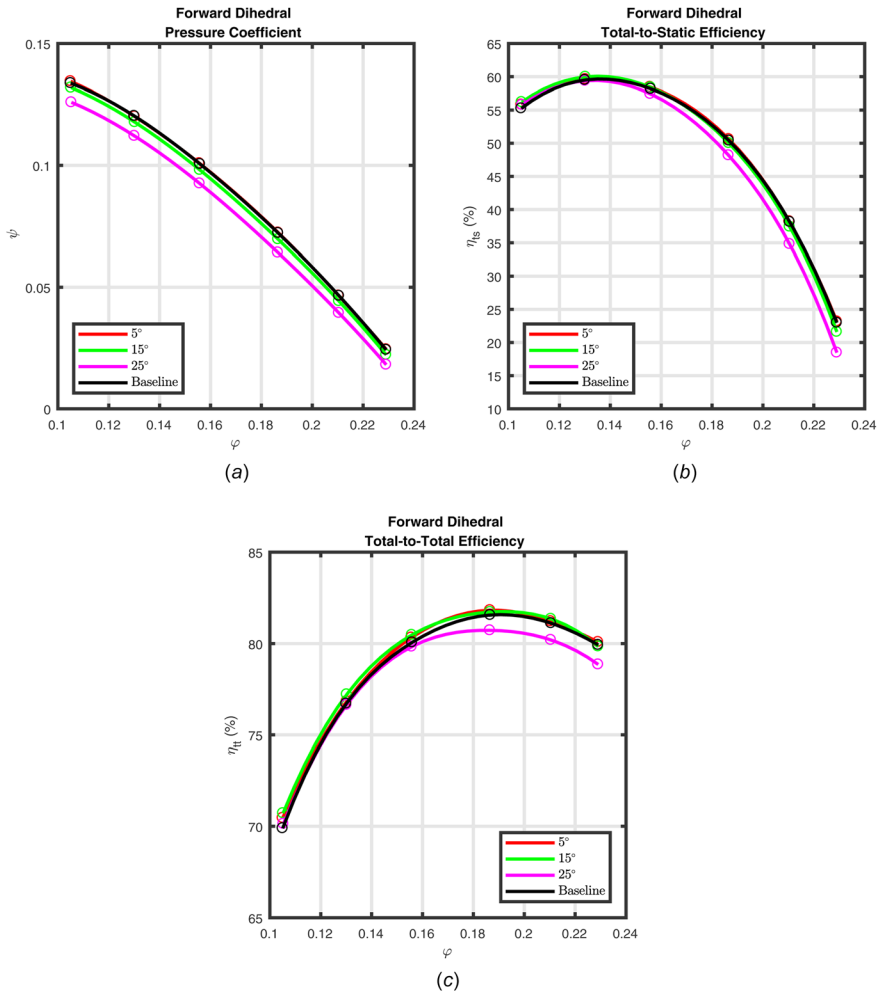

Fig. 12 CFD predictions: comparison between baseline fan and fans with FDH: (*a*) pressure coefficient ψ, (*b*) total-to-static efficiency η_{ts}, and (*c*) total-to-total efficiency η_{tt}: (*a*) $\varphi-\psi$, (*b*) $\varphi-\eta_{ts}$, and (*c*) $\varphi-\eta_{tt}$

4.3 Axial Skew. For axial skew, the blade leans toward the inflow or outflow direction, as described in Sec.1. Investigations on axial skew are not often reported, especially on BAS. According to the results in Secs. 4.1 and 4.2, axial skew is expected to affect the backflow region and hub corner stall.

The predicted aerodynamic performance of fan blades with FAS for different angles is shown in Fig. 15.

For the pressure coefficient ψ, only 5 deg FAS blade gives a small increase at all flow coefficients φ; the others show a drop in ψ. A larger axial skew angle leads to a larger drop; the maximum is 24.6% for 25 deg FAS near $\varphi = 0.23$.

For the total-to-static efficiency η_{ts}, increases are not very significant. The maximum increase is 0.7% for 15 deg FAS at φ near 0.11; the maximum decrease is 4.3% for 25 deg FAS near $\varphi = 0.23$. Near BEP, only the blade with 25 deg FAS gives a decrease; at large φ, decreases are found for all FAS except with 5 deg axial skew angle.

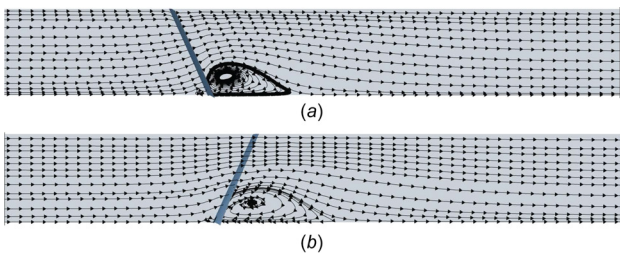

Fig. 13 Comparison of meridional surface streamlines: (*a*) 25 deg FDH and (*b*) 25 deg BDH; both for flow coefficient at BEP

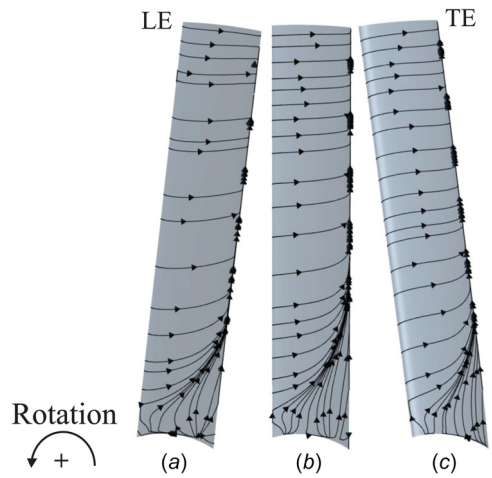

Fig. 14 Boundary layer streamlines near blade suction side surface for (*a*) 25 deg FDH, (*b*) baseline, and (*c*) 25 deg BDH; all for flow coefficient at BEP, "LE" and "TE" stand for leading and trailing edge

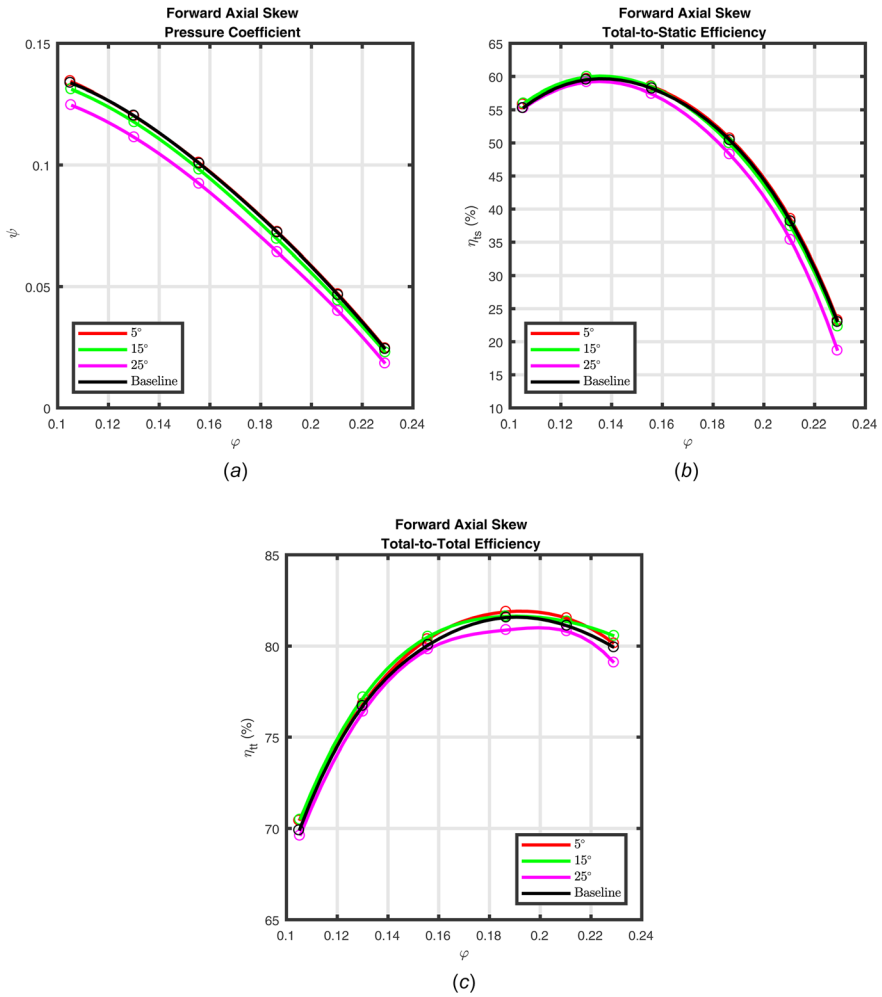

Fig. 15 CFD predictions: comparison between baseline fan and fans with FAS: (*a*) pressure coefficient ψ, (*b*) total-to-static efficiency η_{ts}, and (*c*) total-to-total efficiency η_{tt}: (*a*) $\varphi-\psi$, (*b*) $\varphi-\eta_{ts}$, and (*c*) $\varphi-\eta_{tt}$

For the total-to-total efficiency η_{tt}, improvements are obtained for all angles for all φ, except 25 deg FAS.

The predicted aerodynamic performance of fan blades with BAS for different angles show (data not presented) that the aerodynamic performance is reduced for BAS; larger skew angles give larger decreases. Only 5 deg BAS at large φ gives some increase in ψ and η_{ts}.

The meridional surface streamlines for fan blades with a forward and backward axial skew of 5 deg, 15 deg, and 25 deg are shown in Fig. 16. BAS leads to a backflow region with a larger extent in streamwise direction; the opposite effect occurs with FAS. However, FAS tends to give a larger hub corner stall region upstream of the blades. These observations confirm with the expectation.

4.4 Circumferential Skew. As described in Sec. 1, the advantages and disadvantages of sweep will also be observed with circumferential skew. Therefore, the results in Secs. 4.1 and 4.2 suggest that radial migration boundary layer flow is expected to be reduced by FCS.

The predicted aerodynamic performance of fan blades with FCS at different angles is shown in Fig. 17. The predicted results are qualitatively similar to the results for FSW. No significant improvement is found in both pressure coefficient ψ and total-to-static efficiency η_{ts} over all flow coefficients φ. Some improvements are found in total-to-total efficiency η_{tt} at large φ.

The predicted aerodynamic performance of fan blades with BCS with different angles in Fig. 18 is quite similar to the results with BSW in Sec. 4.1. For pressure coefficient ψ, total-to-static efficiency η_{ts} and total-to-total efficiency η_{tt}, larger skew angles result in larger decreases. For different flow coefficients φ, the drops in ψ and η_{ts} are nearly the same, but for η_{tt} larger decreases are obtained at large φ. However, at a low flow coefficient φ near 0.11, the predicted performance of *BCS* is nearly the same as that of the baseline case, which is different from what is reported for BSW.

The visualization of the boundary layer streamlines on the surface near the blade suction side (data not presented) shows that

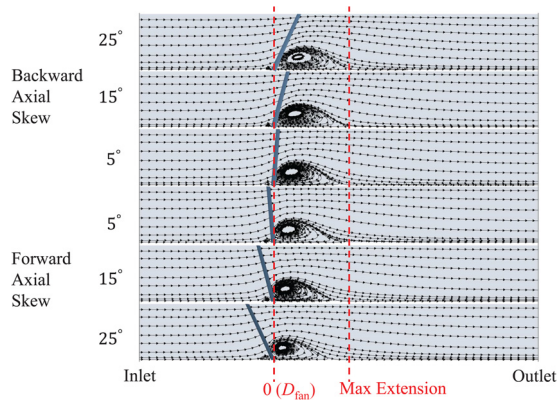

Fig. 16 Backflow region downstream of fan blades with different forward and backward axial skew angles

with FCS the outward flow path near trailing edge is shortened; for BCS the opposite effect is observed.

5 Overview of Skew Effects

In this section, the effects on the aerodynamic performance of sweep, dihedral, and axial and circumferential skew are compared. The focus is on radial migration in Sec. 5.1, the extent of the backflow region in Sec. 5.2, the pressure reduction in Sec. 5.3 and the maximum efficiencies in Sec. 5.4.

5.1 Radial Migration Flow. As discussed in Sec. 4, the boundary layer radial outward flows near the suction side are present for all blades. Differently from the flow patterns in medium to high HTR fans where the radial migration occupies most of the suction side surface (shown, for example, in Ref. [23]), the radial flow in this study is mostly around the hub area and develops toward the tip near the trailing edge.

Blades with FSW and FCS give shortened outward flow paths near the blade suction side surface; BDH also shows such potential (although less noticeable). For BSW and BCS the effect is opposite. However, due to the limited affected area near the suction side surface, such benefits hardly contribute to overall aerodynamic improvements.

5.2 Backflow Region. Blades with FSW and FDH reduce the backflow downstream of the blades, but intensify the hub corner stall region upstream of blades and the separation near the hub blade section; BSW and BDH have the opposite effects.

To quantitatively compare the influence on the backflow region from sweep, dihedral and axial and circumferential skew, the size of the backflow region is quantified by a backflow area percentage $P(z)$ through streamwise (axial) cross section $A(z)$ downstream of the fan blade

$$P(z) = \frac{\int_{A(z)} H(v_z) dA}{\int_{A(z)} dA} \qquad H(v_z) = \begin{cases} 1 & v_z \le 0 \\ 0 & v_z > 0 \end{cases} \tag{6}$$

where v_z is axial velocity. The integrals present in Eq. (6) are numerically evaluated, based on a Delaunay triangulation of the cross section.

The backflow area percentages $P(z)$ are investigated for streamwise locations at $z/D_{\text{fan}} = 0.05$ to $z/D_{\text{fan}} = 0.65$, where the fan is located at $z/D_{\text{fan}} = 0$.

In order to show the most significant trends, the backflow area percentages are shown in Fig. 19 for 25 deg sweep, dihedral, and axial and circumferential skew (both forward and backward).

Compared with the baseline case, blades with forward skew decrease both the size and the axial extent of the backflow region. The opposite holds for blades with backward skew. The effects of

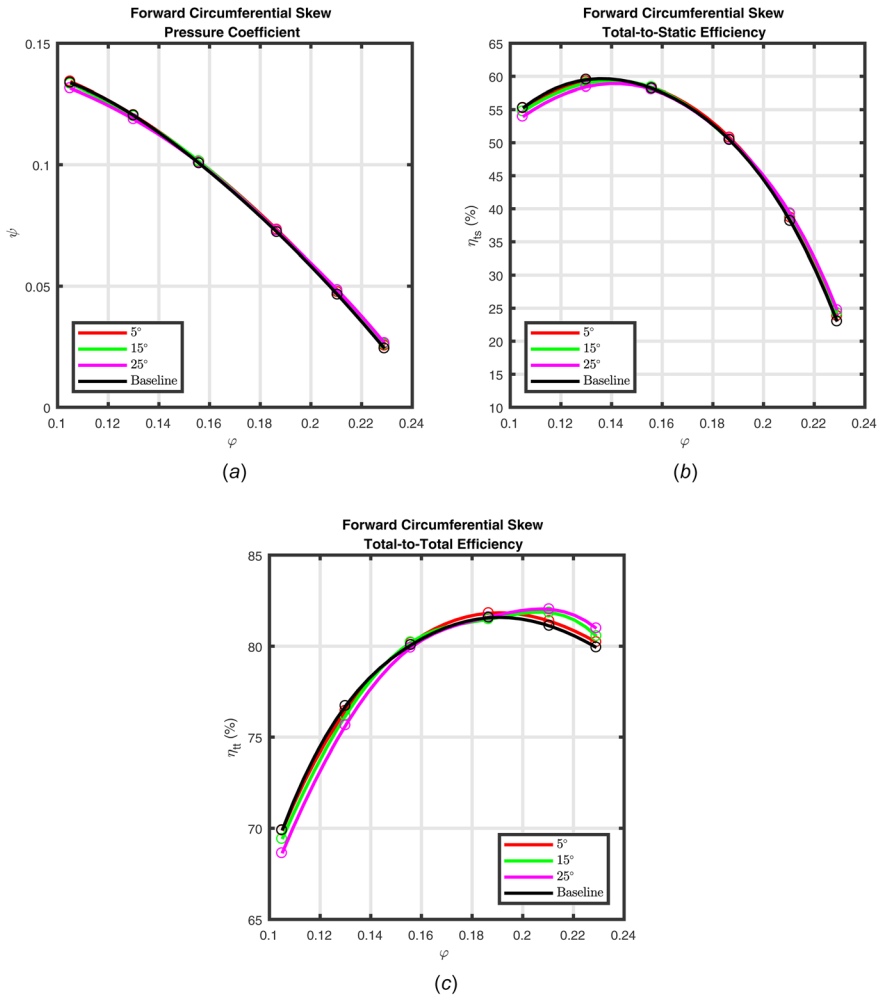

Fig. 17 CFD predictions: comparison between baseline fan and fans with FCS: (*a*) pressure coefficient ψ, (*b*) total-to-static efficiency η_{ts}, and (*c*) total-to-total efficiency η_{tt}: (*a*) $\varphi-\psi$, (*b*) $\varphi-\eta_{ts}$, and (*c*) $\varphi-\eta_{tt}$

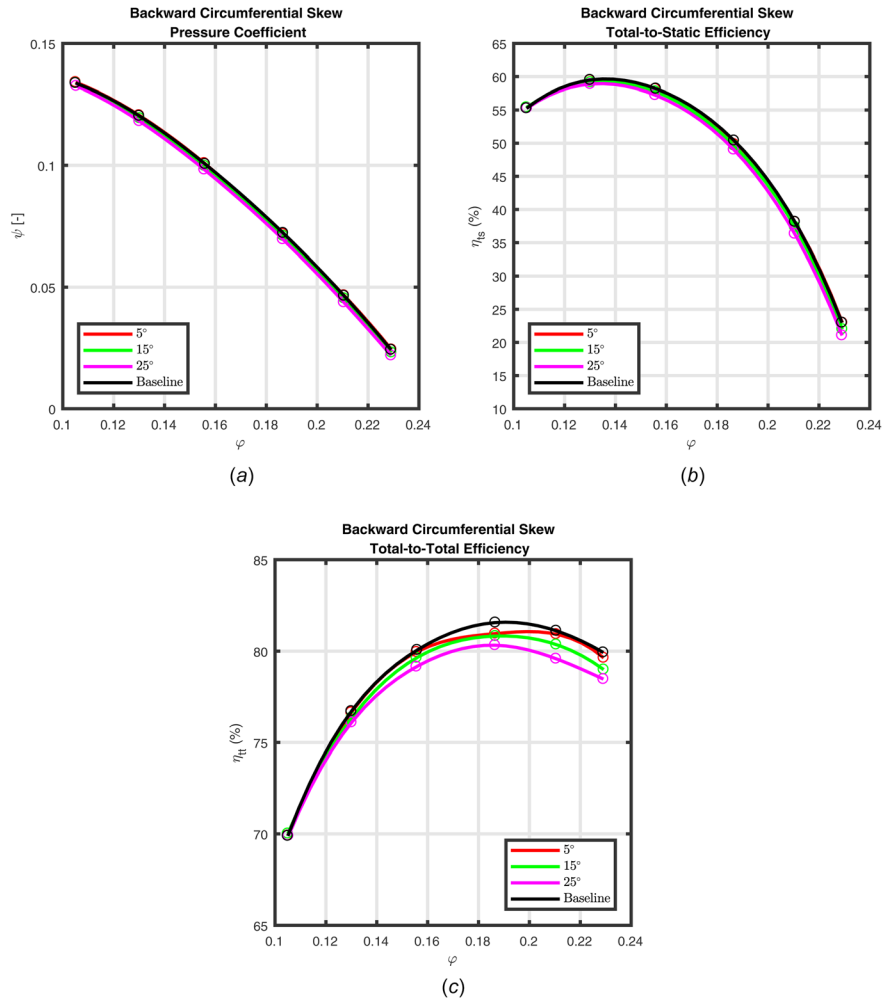

Fig. 18 CFD predictions: comparison between baseline fan and fans with BCS: (*a*) pressure coefficient ψ, (*b*) total-to-static efficiency η_{ts}, and (*c*) total-to-total efficiency η_{tt}: (*a*) $\varphi-\psi$, (*b*) $\varphi-\eta_{ts}$, and (*c*) $\varphi-\eta_{tt}$

sweep and circumferential skew are similar; the same holds for dihedral and axial skew.

In detail, FAS gives the smallest backflow area as well as the smallest axial extent. Blades with BAS give the largest axial extent. The largest backflow area is observed for BSW and BCS.

Since the stagger angle of the investigated fan is $\chi = 15$ deg, circumferential and axial skew participate more in sweep and dihedral, respectively. Hence, circumferential skew plays a main role in the outward radial flow pattern, while axial skew plays the main role in the backflow region and hub corner stall region.

5.3 Pressure Reduction. In investigations of wing aerodynamics [8,10,11] and axial fan aerodynamics [7,13,14], it is shown or assumed that lift/pressure is reduced by $\cos\gamma$ with sweep and by $\cos^2\gamma$ with dihedral. To investigate this effect for fans with small HTR, the pressure coefficient ratios between sweep, dihedral, and the baseline case (ψ/ψ_{Base}) are compared in Fig. 20 for different flow coefficients φ for $\gamma = 25$ deg.

Neither the $\cos\gamma$ effect for sweep nor the $\cos^2\gamma$ effect for dihedral is observed in this study. Backward and forward sweep (the same holds for dihedral) could be expected to give the same pressure reduction, which is not observed. This is different from the results reported in Ref. [14] where the pressure reduction due to forward and backward sweep is reasonably equal (for fans with κ in the range $0.4 - 0.5$). With forward skewed (in the general sense) blades, only FSW gives some increase in pressure coefficient ψ. Overall, the pressure with sweep and dihedral is larger than expected, based on the lift reduction factors of $\cos\gamma$ and $\cos^2\gamma$ for sweep and dihedral from aerodynamics.

These deviations are considered to be due to the flow in axial fans being (much more) three-dimensional (spanwise variations in the angle of attack; hub corner stall and backflow region, etc.) in comparison to flows around wings.

5.4 Predicted Maximum Efficiency. Finally, the potential is investigated for employing sweep, dihedral, and axial and circumferential skew to improve the *maximum* (when varying the flow coefficient φ) total-to-static and total-to-total efficiency; $\eta_{ts,\max} = \max_\varphi \eta_{ts}$ and $\eta_{tt,\max} = \max_\varphi \eta_{tt}$. These maximum efficiencies are shown in Fig. 21.

The results for the maximum total-to-static efficiency $\eta_{ts,\max}$ are shown in Fig. 21(*a*). The highest $\eta_{\text{ts,max}}$ is found for 15 deg FDH (increase by 0.42%). Axial skew and dihedral give almost the same $\eta_{ts,\max}$. For negative angles, axial skew and dihedral give significant decreases in maximum $\eta_{\text{ts,max}}$. Increases in $\eta_{\text{ts,max}}$ are not found with forward sweep and circumferential skew, but then decreases with backward sweep and circumferential skew are smaller.

The results for the maximum total-to-total efficiency $\eta_{tt,\max}$ are shown in Fig. 21(*b*). The highest $\eta_{\text{tt,max}}$ with sweep and circumferential skew is found for the largest considered angle (increases by 0.69% and 0.46%, respectively). For dihedral and axial skew, the optima are found in a forward direction for angles in the range 5 deg–15 deg.

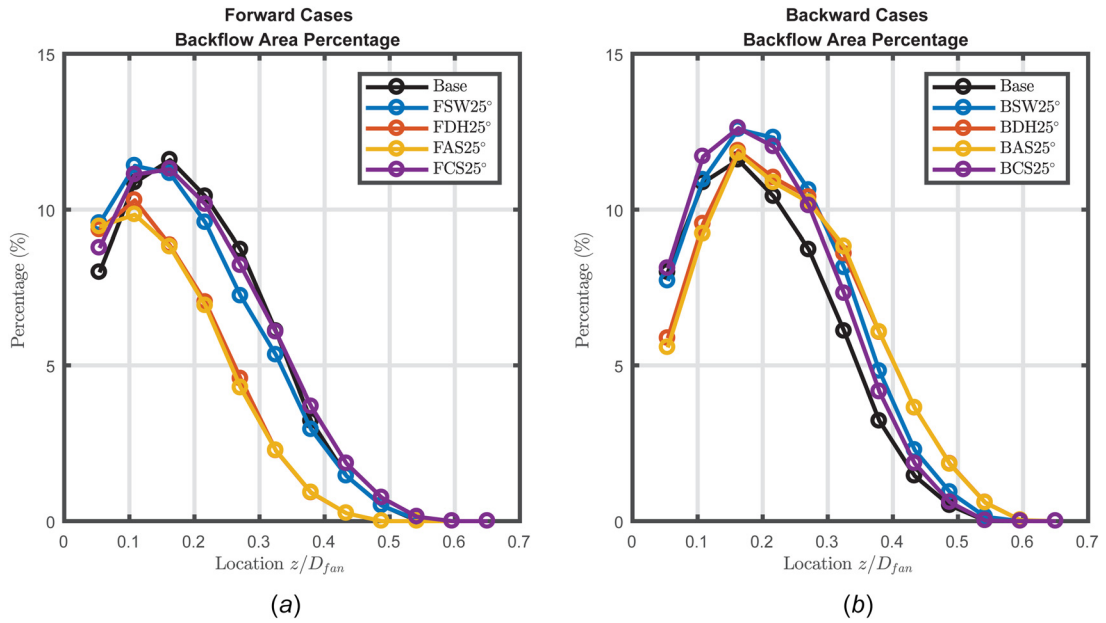

Fig. 19 Backflow percentage *P*(*z*) in Eq. (6) for various axial sections downstream of the blades for $\gamma = 25$ deg: (*a*) forward blades and (*b*) backward blades

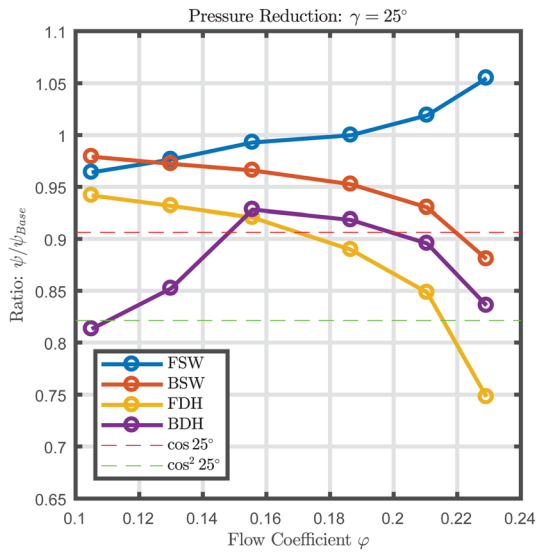

Fig. 20 CFD predictions: pressure reduction ψ/ψ_{Base} due to sweep and dihedral, with $\gamma = 25$ deg; $\varphi-\psi/\psi_{Base}$ with forward and backward sweep and dihedral

6 Conclusions

By using a validated CFD simulation method for low-pressure axial fans with a small hub-to-tip diameter ratio [31], simulations have been performed to investigate the effects of (forward as well as backward) sweep, dihedral, and skew on the aerodynamic performance of such fans, with a linear stacking line.

In contrast to the flow patterns in medium to high HTR fans where radial migration occupies most of the suction side surface, the radial flow in this study is more limited due to the chord of the blade sections being relatively smaller. The beneficial aerodynamic effects of skew (in the general sense) of the blades are therefore more limited here. In general, backward skew gives negative effects, while forward skew can (conditionally) give positive effects.

Blades with sweep hardly lead to improvements in pressure coefficient and total-to-static efficiency. Only at a large flow coefficient does forward sweep result in higher total-to-total efficiency. Forward dihedral gives some improvement in total-to-static and total-to-total efficiency near BEP and for large flow coefficient, but 25 deg FDH and all blades with BDH result in negative effects. Circumferential skew gives a performance similar to that with sweep, in both forward and backward direction, with higher total-to-total efficiency.

It should be noted that the reason for the similar performance in sweep and circumferential skew, as well as with dihedral and axial skew, is the small stagger angle $\chi = 15$ deg. The benefits and disadvantages of sweep and dihedral can be traced to circumferential and axial skew. With different stagger angles, the proportion of circumferential and axial skew in sweep and dihedral is changed, and the consequent performance may also be changed.

Differently from wing aerodynamics where lift coefficients are reduced by factors $\cos\gamma$ and $\cos^2\gamma$ for sweep and dihedral, respectively, the reduction of the pressure coefficients is much more limited (pressure rise is larger than expected). This is considered to be the result of the (much more) complex three-dimensional flow patterns in axial fans, involving backflow and hub corner stall that is absent in flows around wings.

The highest η_{ts} is predicted for axial skew; only 5 deg FAS gives positive effects on both pressure coefficient and efficiency. FAS as well as FDH influence the backflow region significantly, where a larger forward angle helps to suppress the backflow.

Although the improvements from the sweep, dihedral, and skew on fan aerodynamic performance are limited for the considered baseline fan with small HTR, for different optimization purposes, different blade shifts can be applied. FSW and FCS with large angles can be used for higher η_{tt}, while FDH and FAS can suppress backflow and give positive effects on η_{ts}.

For future studies, it is recommended to (i) investigate the effects of sweep, dihedral, and skew with nonstraight stacking line (with angles γ_1, γ_2, γ_3, and γ_4 in Fig. 3 that vary with spanwise locations), aimed at the partial combination of beneficial shape variations into a single blade, (ii) study the effects of the vortex distribution together with sweep, dihedral and skew to obtain better flow control and reduced loss, (iii) perform CFD simulations for other small HTR axial fans with sweep, dihedral and skew, and (iv) perform measurements of small HTR axial fans to investigate the effects of the sweep, dihedral and skew on overall aerodynamic performance as well as local flow phenomena like tip leakage flow.

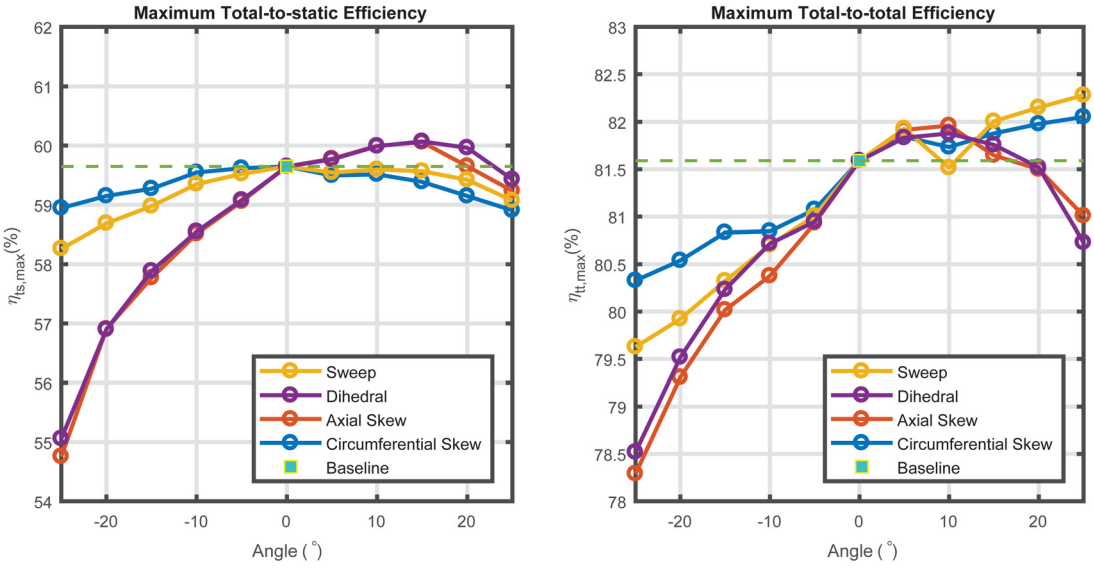

Fig. 21 Predicted *maximum* efficiency for blades with sweep, dihedral and skew, for different (positive and negative) angles: (*a*) total-to-static efficiency $\eta_{ts,max}$, (*b*) total-to-total efficiency $\eta_{tt,max}$: (*a*) skew angle—$\eta_{ts,max}$ and (*b*) skew angle—$\eta_{tt,max}$

Acknowledgment

The authors would like to thank the China Scholarship Council, Howden Netherlands, and Numeca International for support of this research. Peter Holkers and Bastiaan Holm of Howden Netherlands are thanked in particular for valuable discussions.

References

[1] Eck, B., 1973, *Fans: Design and Operation of Centrifugal, Axial-Flow, and Cross-Flow Fans*, Pergamon Press, Oxford, UK.
[2] Wallis, R. A., 1961, *Axial Flow Fans: Design and Practice*, Academic Press, New York.
[3] Dixon, S., 1966, *Fluid Mechanics and Thermodynamics of Turbomachinery*, Butterworth Heinemann, Oxford, UK.
[4] Carolus, T., 2003, *Ventilatoren: Aerodynamischer Entwurf, Schallvorhersage, Konstruktion (in German)*, Springer Verlag, Berlin.
[5] Castegnaro, S., 2018, "Aerodynamic Design of Low-Speed Axial-Flow Fans: A Historical Overview," Designs, **2**(3), p. 20.
[6] Godwin, W. R., 1957, "Effect of Sweep on Performance of Compressor Blade Sections as Indicated by Swept-Blade Rotor, Unswept-Blade Rotor, and Cascade Tests," NACA, Washington, DC, Technical Notes 4062.
[7] Mohammed, K. P., and Raj, D. P., 1977, "Investigations on Axial Flow Fan Impellers With Forward Swept Blades," ASME J. Fluids Eng., **99**(3), pp. 543–547.
[8] Busemann, A., 1935, "Aerodynamischer Auftrieb Bei Überschallgeschwindigkeit," Luftfahrtforschung, **12**(6), pp. 210–220.
[9] Anderson, J., 2016, *Introduction to Flight*, McGraw-Hill Education, New York.
[10] Jones, R. T., 1947, "Effects of Sweepback on Boundary Layer and Separation," NACA, Washington, DC, Report No. Technical Notes 1402.
[11] Maggin, B., and Shanks, R. E., 1946, "The Effect of Geometric Dihedral on the Aerodynamic Characteristics of a 40 Deg Swept-Back Wing of Aspect Ratio 3," NASA Langley Research Centre, Langley Field, Hampton, VA, Report No. 1169.
[12] Smith, L. H. J., and Yeh, H., 1963, "Sweep and Dihedral Effects in Axial-Flow Turbomachinery," ASME J. Fluids Eng., **85**(3), pp. 401–414.
[13] Beiler, M. G., and Carolus, T. H., 1999, "Computation and Measurement of the Flow in Axial Flow Fans With Skewed Blades," ASME J. Turbomach., **121**(1), pp. 59–66.
[14] Masi, M., and Lazzaretto, A., 2015, "A Simplified Theory to Justify Forward Sweep in Low Hub-to-Tip Ratio Axial Fan," ASME Paper No. GT2015-43029.
[15] Gallimore, S. J., Bolger, J. J., Cumpsty, N. A., Taylor, M. J., Wright, P. I., and Place, J. M. M., 2002, "The Use of Sweep and Dihedral in Multistage Axial Flow Compressor Blading-Part I: University Research and Methods Development," ASME J. Turbomach., **124**(4), pp. 521–532.
[16] Gallimore, S. J., Bolger, J. J., Cumpsty, N. A., Taylor, M. J., Wright, P. I., and Place, J. M. M., 2002, "The Use of Sweep and Dihedral in Multistage Axial Flow Compressor Blading-Part II: Low and High-Speed Designs and Test Verification," ASME J. Turbomach., **124**(4), pp. 533–541.
[17] Vad, J., 2008, "Aerodynamic Effects of Blade Sweep and Skew in Low-Speed Axial Flow Rotors at the Design Flow Rate: An Overview," Proc. Inst. Mech. Eng., Part A, **222**(1), pp. 69–85.
[18] Hurault, J., Kouidri, S., Bakir, F., and Rey, R., 2010, "Experimental and Numerical Study of the Sweep Effect on Three-Dimensional Flow Downstream of Axial Flow Fans," Flow Meas. Instrumen., **21**(2), pp. 155–165.
[19] Corsini, A., and Rispoli, F., 2004, "Using Sweep to Extend the Stall-Free Operational Range in Axial Fan Rotors," Proc. Inst. Mech. Eng., Part A, **218**(3), pp. 129–139.
[20] Wadia, A. R., Szucs, P. N., and Crall, D. W., 1998, "Inner Workings of Aerodynamic Sweep," ASME J. Turbomach., **120**(4), pp. 671–682.
[21] Ramakrishna, P. V., and Govardhan, M., 2009, "Combined Effects of Forward Sweep and Tip Clearance on the Performance of Axial Flow Compressor Stage," ASME Paper No. GT2009-59840.
[22] Yamaguchi, N., 1993, "Performance Improvement by Forward-Skewed Blading of Axial Fan Moving Blades," ISABE, **93**(7055), pp. 580–589.
[23] Vad, J., 2012, "Forward Blade Sweep Applied to Low-Speed Axial Fan Rotors of Controlled Vortex Design: An Overview," ASME J. Eng. Gas Turbines Power, **135**(1), p. 012601.
[24] Vad, J., Kwedikha, A. R. A., and Jaberg, H., 2006, "Effects of Blade Sweep on the Performance Characteristics of Axial Flow Turbomachinery Rotors," Proc. Inst. Mech. Eng., Part A, **220**(7), pp. 737–749.
[25] Jang, C.-M., Samad, A., and Kim, K.-Y., 2006, "Optimal Design of Swept, Leaned and Skewed Blades in a Transonic Axial Compressor," ASME Paper No. GT2006-90384.
[26] Seo, S.-J., Choi, S.-M., and Kim, K.-Y., 2008, "Design Optimization of a Low-Speed Fan Blade With Sweep and Lean," Proc. Inst. Mech. Eng., Part A, **222**(1), pp. 87–92.
[27] Denton, J. D., and Xu, L., 1998, "The Exploitation of Three-Dimensional Flow in Turbomachinery Design," Proc. Inst. Mech. Eng., Part C, **213**(2), pp. 125–137.
[28] Sasaki, T., and Breugelmans, F., 1998, "Comparison of Sweep and Dihedral Effects on Compressor Cascade Performance," ASME J. Turbomach., **120**(3), pp. 454–463.
[29] Breugelmans, F. A. H., Carels, Y., and Demuth, M., 1984, "Influence of Dihedral on the Secondary Flow in a Two-Dimensional Compressor Cascade," ASME J. Eng. Gas Turbines Power, **106**(3), pp. 578–584.
[30] Nazmi İlikan, A., and Ayder, E., 2014, "Influence of Dihedral Stacking on the Performance of an Axial Fan," Eng. Appl. Comput. Fluid Mech., **8**(4), pp. 518–529.
[31] Wang, J., and Kruyt, N. P., 2020, "Computational Fluid Dynamics Simulations of Aerodynamic Performance of Low-Pressure Axial Fans With Small Hub-to-Tip Diameter Ratio," ASME J. Fluids Eng., **142**(9), p. 091202.
[32] Airfoil Tools, 2019, "Wortmann Airfoil," Airfoil Tools, accessed July 8, 2019, http://airfoiltools.com
[33] Spalart, P., and Allmaras, S., 1994, "A One-Equation Turbulence Model for Aerodynamic Flows," La Recherche Aérospatiale, **1**, pp. 5–21.